Lamellar Structure of Block Copolymer Poly(oxyethylene–oxypropylene–oxyethylene) in Xylene/Water Mixtures

Guangwei Wu,† Qicong Ying,† and Benjamin Chu*,†,‡

Chemistry Department, State University of New York at Stony Brook, Stony Brook, New York 11794-3400, and Department of Materials Science and Engineering, State University of New York at Stony Brook, Stony Brook, New York 11794-2275

Received February 7, 1994; Revised Manuscript Received June 25, 1994®

ABSTRACT: Synchrotron small angle X-ray scattering (SAXS) was used to study the supramolecular structure formed by a block copolymer, Pluronic L64 ($PEO_{13}PPO_{30}PEO_{13}$), in xylene/water mixtures. Lamellar structure was observed at very high polymer concentrations (e.g., $C^\circ > 0.53$ g/mL). The lamellar spacing was determined by the amount of solubilized water and the copolymer concentration, with the amount of water playing a more important role on the lamellar spacing than the copolymer concentration. The lamellar spacing was almost independent of temperature. However the scattering peak became broader with increasing temperature, implying that the micellar size became smaller. Experimental data could be fitted by the Teubner–Strey model, and the resulting periodicity was in good agreement with the lamellar spacing derived by using the Bragg equation.

Introduction

The gels formed by block copoly(oxyethylene–oxypropylene–oxyethylene) (PEO–PPO–PEO) or block copoly(oxyethylene–oxybutylene–oxyethylene) (PEO–PBO–PEO) could be utilized in controlled drug delivery because of their very low toxicity.[1–4] Studies of this type of gel could go back to the sixties.[5] However, most of the studies on gels formed by PEO–PPO–PEO or PEO–PBO–PEO copolymers in water were focused on the applications.[1–3] Fewer publications dealt with the fundamental aspects.[4,6,7] The structure of such gels and the gelation mechanism remain somewhat obscure because of the composition complexity and the limited techniques which could be used to study them. On the other hand, we now have a reasonable understanding of the aqueous solution behavior of PEO–PPO–PEO or PEO–PBO–PEO copolymers.[4,6–20] In the dilute concentration regime, the micelle formation was determined by the copolymer molar mass, composition, concentration, and temperature. The micelles have a condensed PPO or PBO core and a highly solvated corona. The micellization behavior is similar to that of nonionic surfactants, with the critical micelle concentration decreasing with increasing fraction of the hydrophobic part or with increasing temperature. At semidilute concentrations, the solution behavior became more complicated. The micelles had shape changes, large aggregates could form, and micelle crystallization could be observed.[13–15]

The colloidal behavior of the PEO–PPO–PEO block copolymer in a nonpolar solvent,[12,21–24] which was a good solvent for the middle block, was different because it simulated a switching of the block sequence. The temperature effect on the solubility of the copolymer was opposite to that in an aqueous solution; i.e., the solubility increased with increasing temperature. Micellization had not been observed at and above room temperature even at very high concentrations.[21] However, the micellization process could be induced by adding a small amount of water. The micellar size and shape were strongly influenced by the amount of solubilized water.[22] At high concentrations[23] large secondary aggregates, which were governed by an open-association equilibrium mechanism, coexisted with the smaller micelles and unimers. In this article, the structure of the large aggregates was studied by using synchrotron small angle X-ray scattering at further higher copolymer concentrations where the large aggregates were expected to be dominating species.

Experimental Methods

Materials and Sample Preparation. Pluronic L64 was obtained as a gift from BASF and was used without further purification. The nominal molar mass of this copolymer is 2.9×10^3 g mol^{-1}. Our measured weight-average and number-average molar masses were 3.7×10^3 and 3.4×10^3 g mol^{-1}, respectively.[21] HPLC grade *o*-xylene was purchased from Aldrich Co. and was used as received. A stock solution was prepared by dissolving L64 in *o*-xylene. After having stood for several days, the stock solution was diluted to the required initial concentrations (C°). A calculated amount of clarified distilled water was added to each sample. Then the sample was sealed in a glass vial and kept at ~30 °C for several days in order for the solution to reach equilibrium. The SAXS sample was made by transferring the very viscous sol or gel into an aluminum spacer (~2 mm thick) which had two Kapton windows each with a thickness of 0.001 in. The sealed samples were annealed at ~30 °C for another 2 days in order to remove possible air bubbles. The scattered intensity from different samples was corrected for parameters, such as X-ray intensity variations and detector nonlinearity. However, as all the sample cells had slight variations in thickness, the relative intensity could vary with different samples. This variation did not change the scattered intensity profile which was of our primary interest.

Small Angle X-ray Scattering (SAXS). SAXS experiments were performed at the X3A2 State University of New York (SUNY) Beam Line, National Synchrotron Light Source (NSLS), Brookhaven National Laboratory (BNL). Details about the experimental setup have been described elsewhere.[25] A modified Kratky block collimator system was used along with an OMA photodiode linear position sensitive detector. The X-ray wavelength was set at 0.154 nm. The sample-to-detector distance was 530 (±5) mm. With an incident X-ray beam of about 0.2 × 2 mm, smearing effects on the SAXS profiles were negligible over the q range of interest. The sample temperature was controlled to ±0.02 °C by a precision temperature controller. Routine correction procedures as briefly mentioned in the

* To whom all correspondence should be addressed.
† Chemistry Department.
‡ Department of Materials Science and Engineering.
® Abstract published in *Advance ACS Abstracts*, August 15, 1994.

0024-9297/94/2227-5758$04.50/0

previous section, except for the absolute intensity calibration, were performed on the SAXS data.

Small Angle Neutron Scattering (SANS). SANS experiments were performed with the biology small angle neutron scattering spectrometer[26] located at H9B in the high-flux beam reactor (HFBR) of Brookhaven National Laboratory. Cold neutrons were derived from a solid-hydrogen cold-neutron source located in the beam thimble of the H9B beam line. The wavelength was set at 0.73 nm with a spread in $\Delta\lambda/\lambda$ of less than 10%. Samples were placed in quartz cells and the path length of the sample was 1 mm. A two-dimensional detector was used and the scattered intensity profiles were derived by a circular integration of the two-dimensional pattern. The sample thickness was not exactly the same because the samples were too viscous to fill the entire neutron beam cross section.

Theoretical Background

(a) Fourier Transformations. For a system with spherical symmetry, the X-ray scattered intensity is related to the so-called normalized three-dimensional correlation function by the relation[27]

$$\gamma_3(r) = \frac{1}{Q}\int_0^\infty q^2 I(q)\frac{\sin(qr)}{qr}\,dq \tag{1}$$

where $\gamma_3(r) = \langle\eta(r_1)\eta(r_2)\rangle/\langle\eta^2\rangle$, $r = |r_1 - r_2|$, $\eta(r_i)$ is the local electron density fluctuation at position r_i, and $\langle\eta^2\rangle$ is the mean square electron density fluctuation. The magnitude of the scattering vector $q = (4\pi/\lambda)\sin(\theta/2)$, with λ and θ being respectively the X-ray wavelength and the scattering angle; the invariant Q is defined by the equation

$$Q = \int_0^\infty q^2 I(q)\,dq \tag{2}$$

The assumption of spherical symmetry is not valid for many cases, e.g. lamellar structure. Then the normalized one-dimensional correlation function could be more appropriate, with

$$\gamma_1(r) = \frac{1}{Q}\int_0^\infty q^2 I(q)\cos(qr)\,dq \tag{3}$$

In reality, due to instrument limitation in most cases, the scattered intensity curves are truncated at both the high q and low q ends. To reduce the end effect, both ends are extended on the basis of certain models. In this study, the low q end was made up by using the Debye–Bueche theory

$$I(q) = 8\pi\langle\eta^2\rangle l_p^3/[1 + l_p^2 q^2]^2 \tag{4}$$

where l_p is a correlation length. An extension in the high q region was performed by using the Porod theory

$$I(q) = K_p/q^4 \tag{5}$$

where K_p is a constant related to the surface-to-volume ratio of the phases. In eq 5, we have assumed a sharp interface between water and xylene. This assumption can be tested by making a plot of Iq^4 versus q^4 before background subtraction; a linear behavior over the high q range should support this assumption.

(b) Model Fitting. On the basis of thermodynamic arguments, or by assuming a localized lamellar model, Teubner and Strey[28] proposed a parametric model to fit the scattering behavior of a microemulsion based on the correlation function

$$\gamma(r) = \gamma_o(r)\exp(-r/\xi) \tag{6}$$

where $\gamma_o(r)$ is given by a periodic structure:

$$\gamma_o(r) = (d/2\pi r)\sin(2\pi r/d) \tag{7}$$

After Fourier transformation, it gives

$$I(q) = (8\pi/\xi)\langle\eta^2\rangle c_2/[a_2 + c_1 q^2 + c_2 q^4] \tag{8}$$

The periodicity (d) and the correlation length (ξ) could be extracted from the scattering curve by fitting the three parameters a_2, c_1, and c_2, from which we can compute d and ξ.

$$d = 2\pi\left[\frac{1}{2}\left(\frac{a_2}{c_2}\right)^{1/2} - \frac{1}{4}\frac{c_1}{c_2}\right]^{-1/2} \tag{9a}$$

$$\xi = \left[\frac{1}{2}\left(\frac{a^2}{c_2}\right)^{1/2} + \frac{1}{4}\frac{c_1}{c_2}\right]^{-1/2} \tag{9b}$$

A similar expression has also been derived by Vonk et al.[29] Chen et al.[30] have demonstrated that these two models agree pretty well for some systems.

Results and Discussion

I. Sample Appearance. Three initial L64 concentrations ($C°$ = 0.553, 0.594, and 0.668 g/mL) and four water to EO molar ratios (Z_W = 0.9, 1.3, 1.7, and 2.1) were used in this study. As reported previously,[23] the amount and the size of the large aggregates could be controlled by the copolymer concentration and the water to EO molar ratio (Z_W). The appearances of these samples were different. At low water to EO ratios and copolymer concentrations (e.g., $C°$ = 0.553 g/mL and Z_W = 1.0 and 1.3), the samples were viscous sols, while at higher H_2O/EO ratios and copolymer concentrations (e.g., $C°$ = 0.668 g/mL and Z_W > 1.3), the samples appeared as gels because of their resistance to flow although no definitive tests were made to ascertain the gel state. The sol/gel transition was temperature dependent.

II. Source of SAXS Peaks. Parts a and b of Figure 1 show typical scattering profiles of L64 in xylene/water mixtures at 30.0 °C. There was a peak at $q \sim 0.6$ nm^{-1}. The peak position was shifted only slightly when the water to EO molar ratio changed from 0.9 to 2.1 or the initial copolymer concentration ($C°$) increased from 0.553 to 0.668 g/mL. On the basis of dynamic light scattering experiments,[23] it could be expected that, at the concentrations used in this study, the large aggregates should dominate the scattered intensity. There are two possible sources for the peak: (a) the peak is a result of intraparticle diffraction from the large aggregates; (b) the peak results from a convolution of the structure factor (interparticle interactions) and the large aggregate particle form factor. The samples were very viscous sols or gels, similar to the molten state, implying that the structure factor (interparticle interactions), $S(q,C)$, was close to 1. Therefore, the "diffraction" peaks should be due mainly to the intraparticle structure. Furthermore, the three-dimensional correlation function, obtained by Fourier transformation of the scattered intensity profile, as shown in Figure 2, also suggested that the sample was not totally random, as revealed by the nonexponential decay.[27]

More importantly, we also observed the peaks over the same q range in small angle neutron scattering (SANS) experiments for the same system simply by replacing H_2O with D_2O, as shown in Figure 3. A detailed analysis of the SANS results will be reported later.[24] The scattering length densities[31] of H_2O and of L64 in SAXS are very

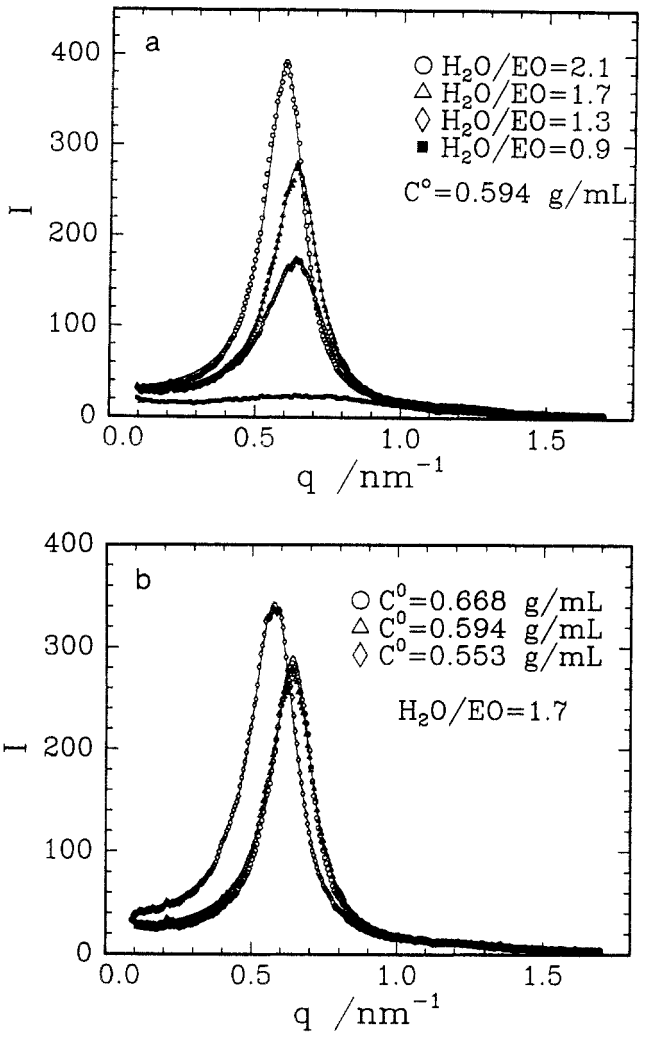

Figure 1. (a) Scattered intensity profiles of L64 in xylene/water mixtures at 30.0 °C. The inserts are the water to EO molar ratio and initial copolymer concentration $C°$. The solid lines are the best fitting curves based on the Teubner–Strey model ($I(q) \propto 1/[a_2' + c_1'q^2 + c_2'q^4]$). (b) Scattered intensity profiles at different copolymer concentrations and a fixed water to EO molar ratio at 30.0 °C. The solid lines are the best fitting curves based on the Teubner–Strey model ($I(q) \propto 1/[a_2' + c_1'q^2 + c_2'q^4]$).

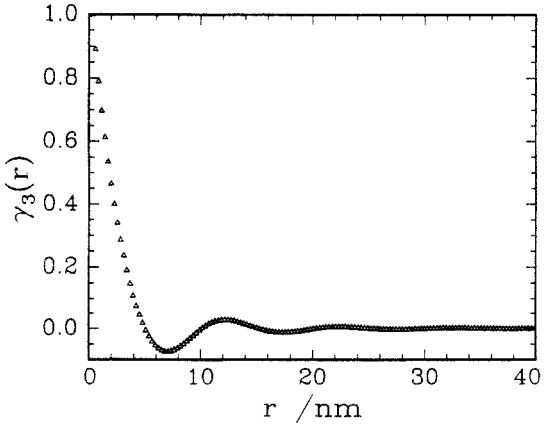

Figure 2. Typical three-dimensional correlation function at 30.0 °C with the initial copolymer concentration ($C°$) and water to EO molar ratio being 0.594 g/mL and 1.7, respectively.

close to each other (9.4 and 9.7 × 10^{10} cm^{-2}, respectively, when compared with 8.1 × 10^{10} cm^{-2} for xylene). The scattering contrast in SAXS came from L64/water and xylene. In the SANS experiment, the scattering length density difference was between D_2O (6.4 × 10^{10} cm^{-2}) and

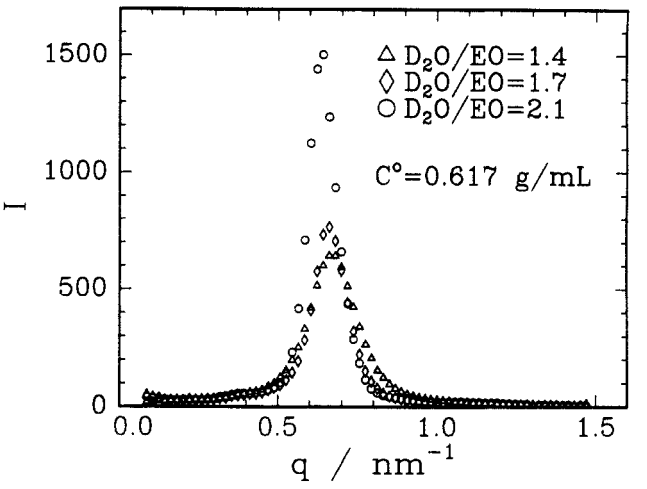

Figure 3. Scattered intensity profile of SANS at different D_2O/EO ratios. Initial L64 concentration $C°$ = 0.617 g/mL. The experimental temperature was 29.0 °C.

L64 (4.6 × 10^9 cm^{-2})/xylene (7.9 × 10^9 cm^{-2}). Due to the contrast difference in SAXS and SANS, the profiles for the form factor $P(q)$ in SAXS and SANS were very different, but the peaks occurred at about the same q value. This observation further confirmed that the scattering peak could be due mainly to diffraction of the intraparticle structure.

III. Structure of Particle. The scattering peaks were taken to come from the diffraction by the large aggregates. The spacing (d) could be estimated by using the Bragg equation:

$$d = 2\pi/q_{max} \tag{10}$$

with q_{max} being the q value at the peak maximum. An estimated value for the spacing (d) was found to be about 10 nm. The hydrodynamic radius, the core radius, and the equivalent hard sphere radius of the micelles were respectively about 9, 5, and 7 nm even at low water to EO ratios.[21] All radii increased with increasing Z_W, implying that the structure of the large aggregates could not be a close-packing of the micelles. The large aggregates could come from a re-association of the micelles. The spacing observed in the SAXS experiments could be interpreted as lamellar in nature (details will be discussed in part VI). After the Lorentz correction (q^2I versus q), there was a shoulder at $\sim 2q_{max}$, as shown in Figure 4a,b. A similar shoulder was observed at $2q_{max}$ by means of SANS after the Lorentz correction, as shown in Figure 5. Thus, the large aggregates had a lamellar structure because the second-order peak was located at $2q_{max}$. We can propose a scenario for the large aggregates as particles having alternative water-rich and oil-rich regions. The low second-order peak intensity could be attributed to the fact that the volume fractions of the two water-rich/oil-rich regions were close to each other because the intensity of the second-order peak was a function of the volume fraction of water-rich phase. The second-order peak should disappear when the volume fraction reached 0.5.

IV. Effect of H_2O/EO Ratio. In order to get the lamellar spacing, three data analysis methods were used: the Bragg equation, the one-dimensional correlation function, and model fitting by the Teubner–Strey model.[28] The lamellar spacing (d) can be derived simply by using the maximum q value after the Lorentz correction based on the Bragg equation (eq 10). The effect of the Lorentz correction on q_{max} was very small for most of the cases because of the sharp peak. Figures 6 and 7 show some

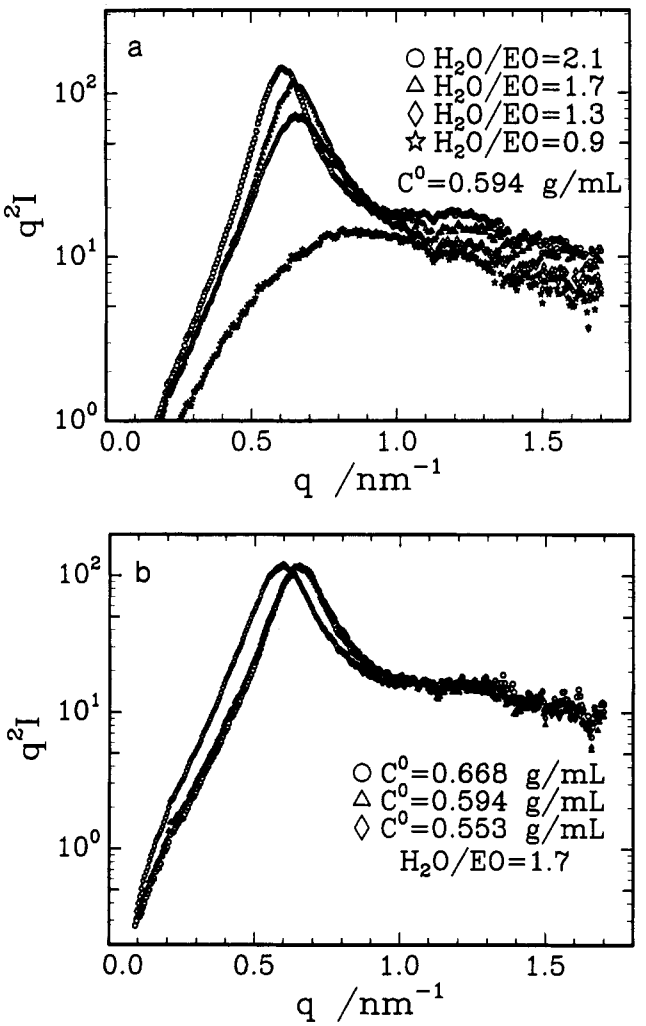

Figure 4. (a) Scattered intensity profiles after Lorentz correction for the same sample conditions as shown in Figure 1a. (b) Scattered intensity profiles after Lorentz correction for the same sample conditions as shown in Figure 1b.

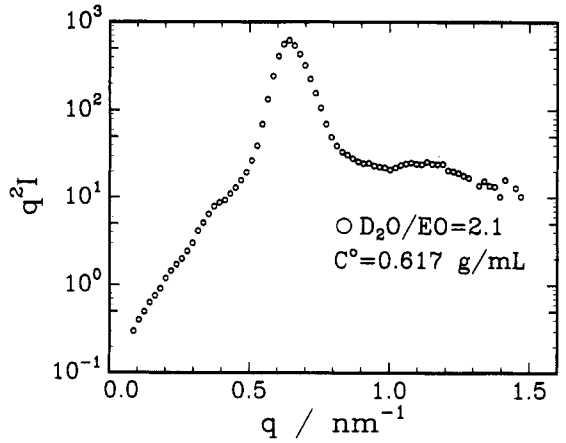

Figure 5. One of the scattered intensity profiles of SANS after Lorentz correction using the same conditions as shown in Figure 3.

typical one-dimensional correlation functions for different H_2O/EO ratios and concentrations. The main characteristic of the one-dimensional correlation functions was that they showed periodicity. The oscillation became weaker with increasing distance. The lamellar spacing (d) could be estimated by the position of the first maximum in the one-dimensional correlation function. The solid lines in Figure 1a,b were best fitting results based on the Teubner–Strey model. Within the q range studied, this

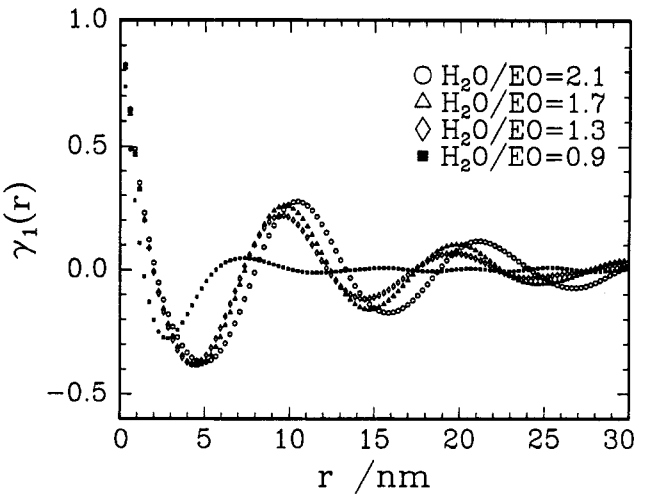

Figure 6. Typical set of one-dimensional correlation functions at 30.0 °C with $C°$ = 0.594 g/mL.

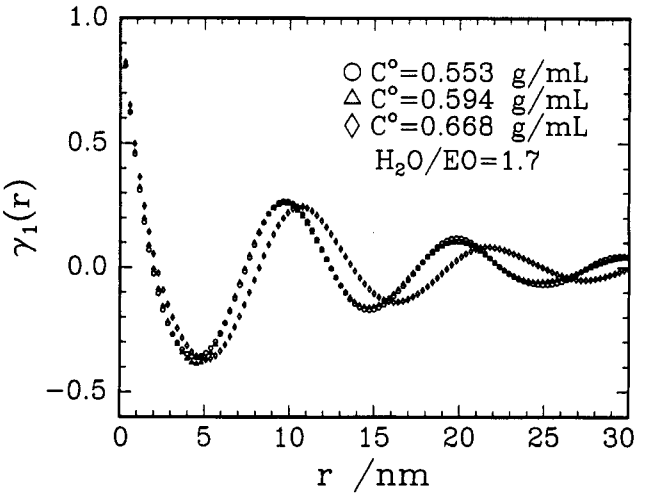

Figure 7. Concentration effect on the one-dimensional correlation function at a fixed water to EO molar ratio (1.7) and 30.0 °C.

model could fit the measured data well. The particle scattering (form) factor decayed to low values in the accessible small q range because of the very large particle size. The diffraction from the lamellar planes should occur at much higher q values because of very short interchain distances. Within the SAXS q range, the scattered intensity was attributed mainly to the diffraction by the interplanes in the direction perpendicular to the lamellar plane. The alternating arrangement of water and oil domains and the loss of long range order were fulfilled by the system studied.

The spacing (d) as a function of H_2O/EO ratio is shown in Figures 8 and 9. The lamellar spacings (d) derived from the three approaches were essentially the same to within the experimental error limits, as shown in Figure 8. This agreement indirectly supports the large aggregates to have a lamellar structure because the lamellar structure was assumed in the one-dimensional correlation approach. The spacing increased with increasing H_2O/EO ratio over a range of copolymer concentrations. The d values decreased slightly with increasing copolymer concentration.

With the lamellar structure, the volume (V) occupied by L64, water, and xylene, the spacing (d), and the average cross-section area (S) of each L64 molecule are related as follows:

$$V = V_{L64} + V_{wat} + V_{xyl} = Sd \qquad (11)$$

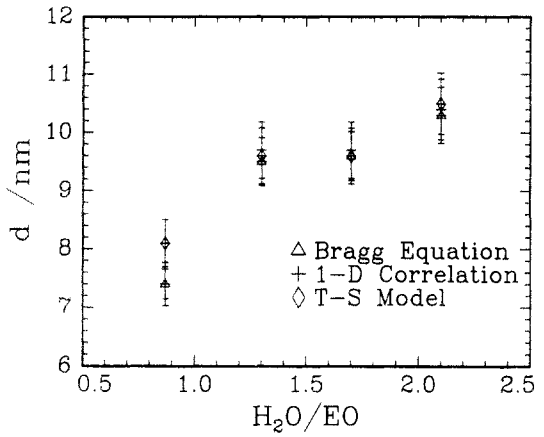

Figure 8. Comparison of direct analysis (Bragg equation), the one-dimensional correlation function, and Teubner–Strey model fitting. $C°$ = 0.594 g/mL, and the experimental temperature was 30.0 °C.

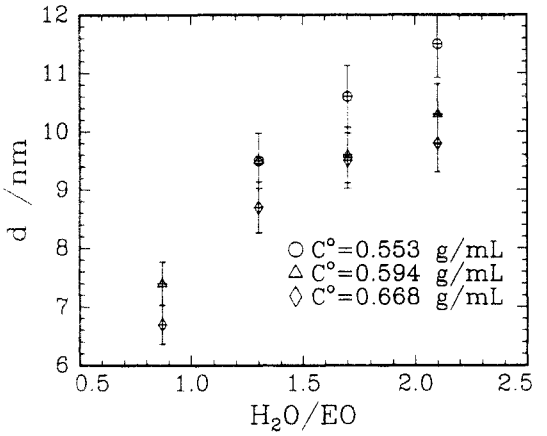

Figure 9. Lamellar spacing as a function of the water to EO molar ratio at three different copolymer concentrations and 30.0 °C.

where V_{L64}, V_{wat}, and V_{xyl} are the volume of each L64 molecule, of inherent water, and of xylene, respectively. On the basis of the measured weight-average molar mass of L64 (3.7×10^3 g/mol), V_{L64} was estimated to be 5.9 nm^3. The volumes of inherent water and xylene were related to V_{L64} by the molar ratio of H_2O/EO (Z_W) and xylene/PO (Z_X) by the equations

$$V_{wat} = 0.172 V_{L64} Z_W \tag{12a}$$

and

$$V_{xyl} = 1.32 V_{L64} Z_X \tag{12b}$$

where the coefficients are the conversion factors which relate the molar ratio to the volume ratio. For example, $V_{wat}/V_{L64} = Z_W(M_W/d_W)/(M_{EO}/d_{EO}/0.4) = 0.172 Z_W$, where M and d represent molecular weight and density, respectively, and the 0.4 is the weight fraction of EO in L64. By combination of eq 11 with eqs 12a and 12b, eq 11 could be expressed as

$$V_{L64}(1 + 0.172 Z_W + 1.32 Z_X) = Sd \tag{13}$$

Qualitatively, the higher the copolymer concentration, the lower the Z_X. If the cross-section area remained unchanged at a fixed H_2O/EO value (Z_W), the spacing (d) should decrease with increasing copolymer concentration, in agreement with the observed result. From eq 13, we could see that the contribution of solubilized water to the total

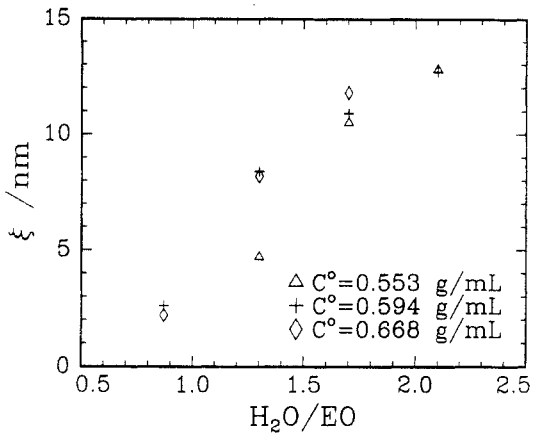

Figure 10. Correlation length obtained from model fitting as a function of the water to EO molar ratio at different copolymer concentrations and 30.0 °C.

volume (V) was very limited; e.g., the volume (V) increased about 10% when Z_W changed from 0.9 to 2.1 with the assumption that Z_X was equal to 0.5. An increase in the lamellar spacing with increasing Z_W could not be explained only by the volume change caused by the solubilized water. At a fixed copolymer concentration ($C°$), it would be unlikely that the xylene to PO ratio (Z_X) increased with increasing Z_W. The only possible explanation should be that the cross-section area (S) decreased with increasing Z_W. It was very difficult to decide what the exact value of Z_X should be because some of the xylene molecules might not be attached to the copolymer. At the highest Z_W value (2.1), the samples at three different copolymer concentrations all appeared to be in the gel state. To the first-order approximation and as an upper limit, the Z_X value in the large aggregates might be assumed to be the same as that in the small particles, i.e., all particles having the same Z_X value, of 0.68, 0.58, and 0.43 for $C°$ = 0.557, 0.594, and 0.668 g/mL, respectively. Thus, the calculated cross-section areas (S) of each L64 molecule were 1.16, 1.20, and 1.17 nm^2 for $C°$ = 0.553, 0.594, and 0.668 g/mL, respectively. The S values were essentially unaffected by the initial copolymer concentration and were very close to the cross-section area at the air/water interface of nonionic surfactants (0.5 nm^2)[32] and Pluronic P94 (1.28 nm^2),[19] but were much smaller than the cross-section area at micellar core/corona interface in the dilute solution regime (2.0 nm^2).[21] Qualitatively, the S value decreased with increasing Z_W. The interfacial energy could be responsible for the decrease in S. Our result could further support the argument that the interfacial energy was the driving force for the micellar shape change.[22]

The correlation length (ξ) could be related to the extension of the alternative structure and represented an indication of the size for the large aggregates. The larger the ξ value, the larger the aggregate size. Figure 10 shows the correlation length (ξ) as a function of water to EO ratio. The correlation length increased with increasing water to EO ratio, suggesting that the size of the large aggregates increased with increasing water to EO ratio, in agreement with the dynamic light scattering (DLS) results.[23]

V. Temperature Effect. DLS experiments showed that the size and the amount of the large aggregates decreased with increasing temperature. Although the amount and the exact size of the large aggregates could not be determined by this set of SAXS experiments because of the relative intensity scaled and the limited experimental q range, the change in the size of the large

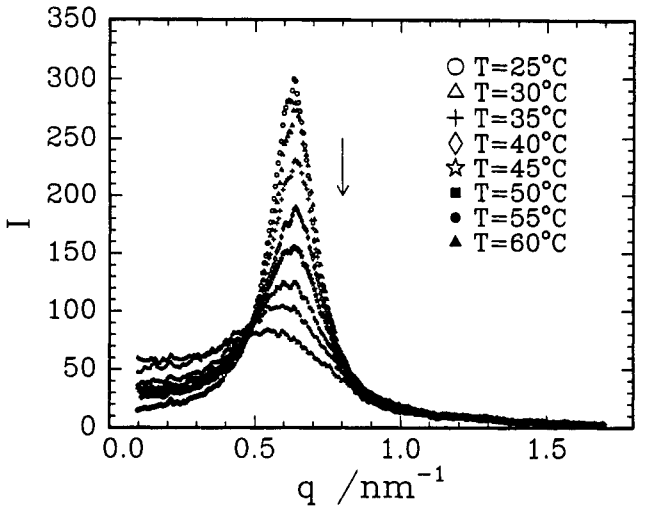

Figure 11. Temperature effect on the scattered intensity profile at a high water to EO molar ratio (1.7). $C°$ = 0.594 g/mL.

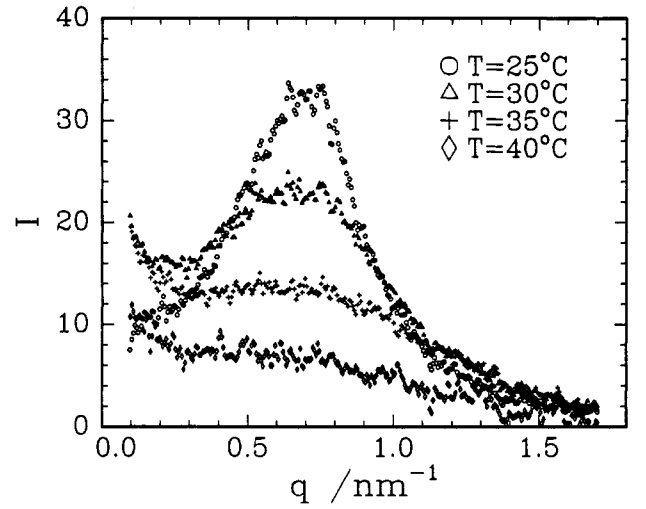

Figure 12. Temperature effect on the scattered intensity profile at a low water to EO molar ratio of 0.9. $C°$ = 0.594 g/mL.

aggregates could be determined by measuring the change in the SAXS peak half-width and some other parameters. The temperature dependence of a typical scattered intensity profile is shown in Figure 11. With increasing temperature, the peak position remained almost unchanged, the peak intensity decreased, the peak became broader, and the scattered intensity in the low q limit increased at higher water to EO ratios, e.g., $Z_W > 1.7$. At a low water to EO ratio, e.g., at $Z_W = 0.9$, the peak disappeared at high temperatures, as shown in Figure 12. Figure 13 shows the temperature dependence of the scattered intensity profile after the Lorentz correction. The peak position remained unchanged, implying that the lamellar spacing remained unchanged within the temperature range used in this study (25–60 °C). Both the decrease in the peak scattered intensity and the broadening of the peak suggested that the size of the large aggregates decreased with increasing temperature. An increase in the scattered intensity at low q values also implied that the intensity contribution by the small particles increased with increasing temperature. At low water to EO ratios, the contribution of the small particles became dominated at high temperatures and the peak attributed to the large particles could no longer be observed. The results were in good agreement with those from DLS measurements.[23] The temperature effect on the one-dimensional correlation function is shown in Figure

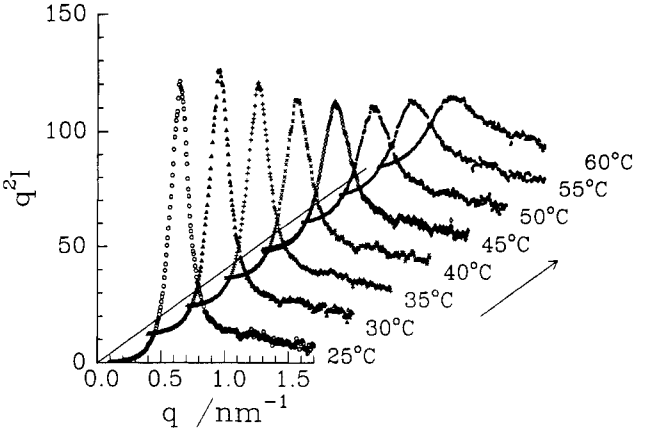

Figure 13. Typical set of scattered intensity profiles after Lorentz correction at different temperatures. The copolymer concentration and water to EO ratios were the same as in Figure 11.

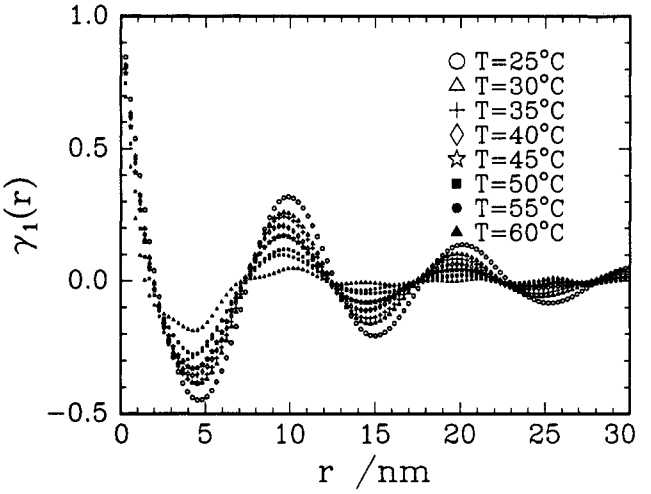

Figure 14. One-dimensional correlation function obtained by Fourier transformation of the scattered intensity profiles in Figure 11.

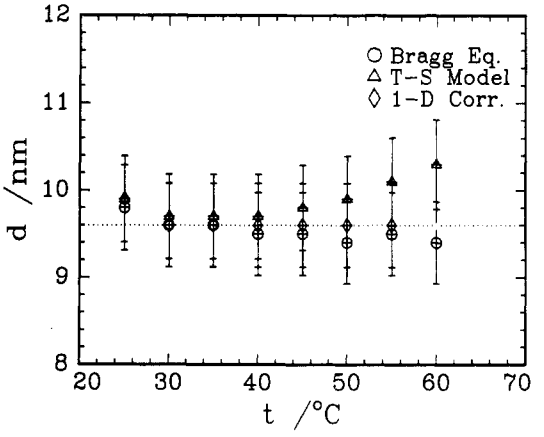

Figure 15. Lamellar spacing d as a function of temperature at $C°$ = 0.594 g/mL and Z_W = 1.7. The three symbols represent values obtained by three different data analysis approaches. The horizontal dashed line is used as a guide.

14. The peak positions remained almost unchanged when the temperature was varied from 25 to 60 °C. The oscillation diminished much faster at higher temperatures, implying that the size of the large aggregates decreased with increasing temperature.

Figure 15 shows the lamellar spacing as a function of temperature (t/°C). The lamellar spacing remained almost unchanged, and the results from the three approaches

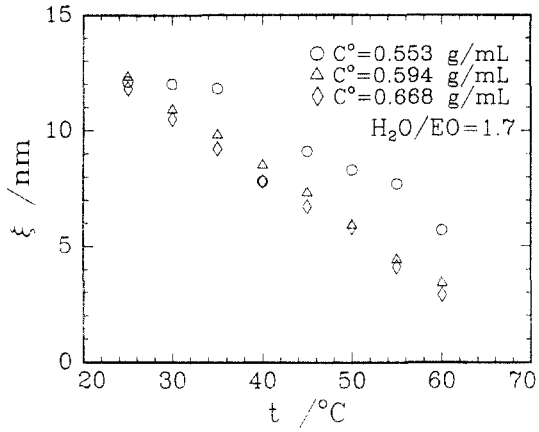

Figure 16. Correlation length obtained from model fitting as a function of temperature at different copolymer concentrations.

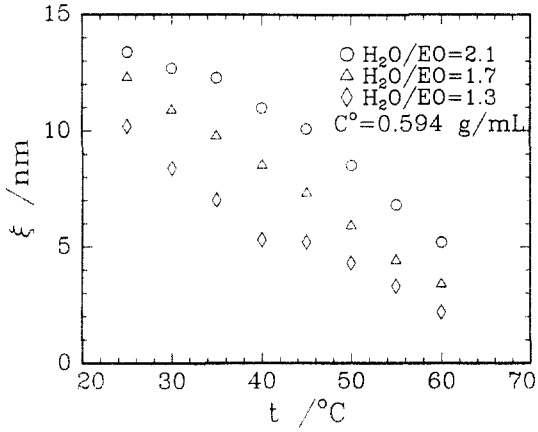

Figure 17. Correlation length obtained from model fitting as a function of temperature at different water to EO molar ratios.

agreed fairly well. At high temperatures, the Teubner–Strey model deviated slightly from the other two approaches. A possible reason could be that the scattered intensity contribution from small particles increased with increasing temperature. The scattered intensity profile became a mixture of the contributions of the large and the small particles at high temperatures. Therefore, the assumption for the correlation function used in the Teubner–Strey model deviated from the experiment. The correlation length obtained from model fitting as a function of temperature is shown in Figures 16 and 17. Over the copolymer concentration and the water to EO ratio range studied, the correlation length decreased with increasing temperature, implying that the size of the large aggregates decreased with increasing temperature, in agreement with the observation that the SAXS scattered intensity peak broadened and the oscillation in the one-dimensional correlation functions became diminished faster with increasing temperature.

VI. Conformation of Polymer Chain in the Large Aggregates. The conformation of the copolymer chains in the large aggregates could be complex. Based on the information obtained from SAXS, some idea about the conformation could be extracted. With the assumption that there was a relatively sharp boundary between the PEO plus water-rich region and the PPO plus xylene-rich region, the thickness of PEO plus water-rich region (d_{PEO}) could be estimated by the relation

$$d_{PEO} = d\varphi_{PEO} \tag{14}$$

where φ_{PEO} was the volume fraction of PEO plus water-rich region. As a low limit of d_{PEO} and to the first-order approximation, the sample composition was used to calculate the φ_{PEO} value. This approximation could be close to the real situation at high water to EO ratios (e.g., 2.1) because the samples were then in the gel state. The calculated spacings of the PEO plus water-rich region (d_{PEO}) were 3.9, 3.7, and 3.9 nm, respectively, for $C°$ = 0.553, 0.594, and 0.668 g/mL. The d_{PEO} values from the three concentrations were essentially the same, implying that the approximation was reasonable. For Pluronic L64, the stretched block length could be estimated by assuming a certain chain conformation. For the PEO block, there are three possible conformations: zigzag,[33] helix,[34] and meander.[33] The stretched PEO block length is about 5.6, 4.2, and 3.1 nm for the zigzag, helix, and meander conformations, respectively (based on the number-average molar mass of L64, 3.4×10^3 g/mol). Two conclusions could be deduced from a comparison of the values of d_{PEO} between experiment and theoretical calculations: (1) the PEO block was interpenetrated in the large aggregates, and (2) the conformation of the PEO block was most likely helical. As mentioned previously, the cross-section area of each L64 molecule was around 1.2 or 0.6 nm^2 per chain because there were two PEO blocks in each molecule. This value was very close to the values of the cross-section area in the air/water interface of nonionic surfactant molecules[32] or Pluronic P94 chains.[19] In other words, the PEO blocks were rather close-packed in the large aggregates. Therefore, it was possible that the PEO chains took the same conformation in the large aggregates as in the crystalline state, i.e., the helix conformation.[34] The crystallization of PEO in copolymers (e.g., PEO–PS) in the presence of a good solvent for the PEO block has been reported,[35] indirectly supporting our results.

The thickness of the PPO plus xylene-rich region (d_{PPO}) could be related to the copolymer concentration. With the approximation used in the previous paragraph, d_{PPO} was equal to 7.6, 6.6, 5.9 nm, respectively, for $C°$ = 0.553, 0.594, and 0.668 g/mL. The conformation of the PPO chains was more complex. It is unlikely that the PPO chain has a helix conformation because of the steric effect of the methyl group. PPO is also much more difficult to crystallize when compared with PEO. Both the zigzag conformation with a loop (both PEO blocks located at the same layer with a stretched length of 6.3 nm) and the meander-like conformation (two PEO blocks located at different layers with a stretched length of 7.0 nm) could fit the spacing of the PPO plus xylene region. Thus, the PPO chain conformation could not be ascertained on the basis of the available data.

Conclusions

The structure formed by L64 in xylene/water mixtures was studied by synchrotron small angle X-ray scattering (SAXS) over a temperature range 25–60 °C. Direct analysis (Bragg equation), one-dimensional Fourier transformation, and model fitting (Teubner–Strey model) were used in the SAXS data analysis. The agreement among the three approaches was quite good. Based on the obtained results, the following conclusions could be reached.

(1) The large aggregates had a lamellar structure. The lamellar spacing was controlled mainly by the water to EO ratio. The size of the large aggregates and the lamellar spacing increased with the increasing water to EO molar ratio. The effect of copolymer concentration on the lamellar spacing was small when compared with the effect of water.

(2) The lamellar spacing was almost unaffected by temperature within the investigated temperature range. The size of the large aggregates decreased with increasing temperature, as indicated by peak broadening and a decrease in the correlation length.

(3) The polymer chains were rather close-packed in the large aggregates. The cross-section area of each polymer chain was around 60 Å^2, which was close to the value of the cross-section area for nonionic surfactants[32] or Pluronic P94[19] at the water/air interface. In the large aggregates, the PEO blocks of L64 could have a helical conformation.

Our results on the large aggregates as revealed by SAXS were in very good agreement with the dynamic light scattering results[23] at slightly lower copolymer concentrations.

Acknowledgment. We gratefully acknowledge support of this research by the U.S. Army Research Office (DAAH0494G0053), the Polymers Program (DMR-9301294), Division of Material Research, National Science Foundation and the Department of Energy (Grant DEFG0286ER45237.010), as well as the SUNY Beamline at the National Synchrotron Light Source, Brookhaven National Laboratory. We thank Dieter Schneider at BNL for his very helpful assistance on the SANS experiment.

References and Notes

(1) Schmolka, I. R. In *Polymers for Controlled Drug Delivery*; Tarcha, P. J., Ed.; CRC Press: Boston, 1992.
(2) Lundsted, L. G.; Schmolka, I. R. In *Block and Graft Copolymerization*; Ceresa, R. J., Ed.; John Wiley & Sons: New York, 1975; Vol. II.
(3) Chen-chow, P.-C.; Frank, S. G. *Int. J. Pharm.* **1981**, *8*, 89.
(4) Luo, Y.; Nicholas, C. V.; Attwood, D.; Collett, J. H.; Price, C.; Booth, C.; Chu, B.; Zhou, Z. *J. Chem. Soc., Faraday Trans.* **1993**, *89*, 539.
(5) Schmolka, I. R. *Am. Perfum. Cosmet.* **1967**, *82*, 25.
(6) Brown, W.; Schillén, K.; Almgren, M.; Hvidt, S.; Bahadur, P. *J. Phys. Chem.* **1991**, *95*, 1850.
(7) Wanaka, G.; Hoffmann, H.; Ulbricht, W. *Colloid Polym. Sci.* **1990**, *268*, 101.
(8) Zhou, Z.; Chu, B. *J. Colloid Interface Sci.* **1988**, *126*, 171.
(9) Zhou, Z.; Chu, B. *Macromolecules* **1987**, *20*, 3089; **1988**, *21*, 2548.
(10) Tontisakis, A.; Hilfiker, R.; Chu, B. *J. Colloid Interface Sci.* **1990**, *135*, 427.
(11) Schillén, K.; Brown, W.; Koňák, C. *Macromolecules* **1993**, *26*, 3611.
(12) Chu, B.; Zhou, Z.; Wu, G. *J. Non-Cryst. Solids*, in press.
(13) Brown, W.; Schillén, K.; Hvidt, S. *J. Phys. Chem.* **1992**, *96*, 6038.
(14) Mortensen, K.; Brown, W. *Macromolecules* **1993**, *26*, 4128.
(15) Mortensen, K. *Europhys. Lett.* **1992**, *19*, 599.
(16) Yu, G.-E.; Deng, Y.; Dalton, S.; Wang, Q.-C.; Attwood, A.; Price, C.; Booth, C. *J. Chem. Soc., Faraday Trans.* **1992**, *88*, 2537.
(17) Linse, P.; Malmsten, M. *Macromolecules* **1992**, *25*, 5434.
(18) Malmsten, M.; Lindman, B. *Macromolecules* **1992**, *25*, 5440.
(19) Bahadur, P.; Pandya, K. *Langmuir* **1992**, *8*, 2666.
(20) Linse, P. *Macromolecules* **1993**, *26*, 4437.
(21) Wu, G.; Zhou, Z.; Chu, B. *Macromolecules* **1993**, *26*, 2117.
(22) Wu, G.; Zhou, Z.; Chu, B. *J. Polym. Sci., Polym. Phys. Ed.* **1993**, *31*, 2035.
(23) Wu, G.; Chu, B. *Macromolecules* **1994**, *27*, 1766.
(24) Chu, B.; Wu, G.; Schneider, D. *J. Polym. Sci. Polym. Phys.*, accepted for publication.
(25) Chu, B.; Wu, D.; Wu, C. *Rev. Sci. Instrum.* **1987**, *58*, 1158.
(26) Schneider, D. K.; Schoenborn, B. P. In *Neutrons in Biology*; Schoenborn, B. P., Ed.; Plenum: New York, 1984; p 119.
(27) *Small Angle X-ray Scattering*; Glatter, O., Kratky, O., Eds.; Academic Press: London, 1983.
(28) Teubner, M.; Strey, R. *J. Chem. Phys.* **1987**, *87*, 3195.
(29) Vonk, C. G.; Billman, J. F.; Kaler, E. W. *J. Chem. Phys.* **1988**, *88*, 3970.
(30) Chen, S.-H.; Chang, S.-L.; Strey, R. *J. Chem. Phys.* **1990**, *93*, 1907.
(31) *Structure Analysis by Small-Angle X-Ray and Neutron Scattering*; Feigin, L. A., Svergun, D. I., Eds.; Plenum Press: New York, 1987.
(32) Ravey, J. C.; Buzier, M. In *Surfactant in Solution*; Mittal, K. L., Lindman, B., Eds.; Plenum Press: New York, 1984.
(33) Rosch, H. In *Nonionic Surfactants*; Shick, M. J., Ed.; Dekker: New York, 1967.
(34) Tadokoro, H. *Macromol. Rev.* **1967**, *1*, 119.
(35) Gallot, B. *Adv. Polym. Sci.* **1978**, *79*, 85. Gallot, B. In *Liquid Crystaline Orders in Polymers*; Blumstein, A., Ed.; Academic Press: New York, 1978.